Available online at www.sciencedirect.com
SCIENCE DIRECT®
Journal of Power Sources 119–121 (2003) 799–804
JOURNAL OF POWER SOURCES
www.elsevier.com/locate/jpowsour

A comparison among $LiPF_6$, $LiPF_3(CF_2CF_3)_3$ (LiFAP), and $LiN(SO_2CF_2CF_3)_2$ (LiBETI) solutions: electrochemical and thermal studies

J.S. Gnanaraj[a], E. Zinigrad[a], M.D. Levi[a], D. Aurbach[a,*], M. Schmidt[b]

[a]*Department of Chemistry, Bar-Ilan University, Ramat-Gan 52900, Israel*
[b]*Merck KGaA, D-64293 Darmstadt, Germany*

Abstract

EC–DMC–DEC solutions comprising $LiPF_3(CF_2CF_3)_3$ (LiFAP), $LiPF_6$ and $LiN(SO_2CF_2CF_3)_2$ (LiBETI) were tested with graphite and $LiMn_2O_4$ electrodes. Cyclic voltammetry (CV, fast and slow scan rates), chronopotentiometry, impedance spectroscopy, surface sensitive FTIR and XPS were used for this study. It was found that the new salt LiFAP is a promising candidate for use in rechargeable Li-ion batteries. The thermal behavior of these electrolyte solutions was also studied using accelerating rate calorimetry (ARC). It was found that LiFAP solutions are more stable than $LiPF_6$ solutions while LiBETI solutions have the highest thermal stability.

Keywords: $LiPF_6$; $LiPF_3(CF_2CF_3)_3$ (LiFAP); $LiN(SO_2CF_2CF_3)_2$ (LiBETI); Thermal stability; ARC; Impedance spectroscopy; Surface films; Li-ion batteries

1. Introduction

In recent years, we see permanent efforts to improve performance of Li-ion batteries so they can be used as power sources for electric vehicles (EV) and other large-sized equipment [1]. However, large-size Li-ion batteries are not yet used in practice due to safety considerations. When the temperature of lithium-ion batteries is raised as a result of abusive conditions, a process of self-heating can be initiated. The organic compounds used as solvents in Li-ion cells are flammable and therefore, the danger of heat generation by chemical decomposition and possible thermal runaway of Li-ion batteries in abuse cases are important factors to be considered.

The most popular salt, $LiPF_6$, used in Li-ion batteries suffers from thermal instability and decomposes to LiF and PF_5 [2]. The latter species react readily with protic substances (H_2O, ROH, surfaces with –OH groups such as glass) to form PF_yO_x compounds and HF [3]. Hence, HF is unavoidably present in all $LiPF_6$ solutions. This acidic contaminant is reduced on the lithiated graphite surfaces, reacts with protective surface films, which are formed on the Li–C anodes, and also reacts with the Li_xMO_y cathode materials to form inactive phases on the surfaces of the cathode particles [4]. Recently, Schmidt et al. [5] have reported on a new salt (LiFAP–$LiPF_3(CF_2CF_3)_3$) with relatively stable P–F bonds. Here we present comparative electrochemical and surface chemistry studies of graphite anodes and $LiMn_2O_4$ spinel cathodes in electrolyte solutions of $LiPF_6$, LiFAP, and $LiN(SO_2CF_2CF_3)_2$ (LiBETI) in EC–DMC–DEC mixtures. The thermal behavior of these solutions was studied using accelerating rate calorimeter (ARC) and differential scanning calorimetry (DSC).

2. Experimental

The electrolyte solutions used were 1 M LiFAP, 1 M $LiPF_6$, and 1 M $LiN(SO_2CF_2CF_3)_2$ in a ternary solvent mixture EC + DEC + DMC (2:1:2) from Merck KGaA (highly pure solutions, Li battery grade, could be used as received). All the work was performed under a highly pure argon atmosphere in standard glove boxes from VAC Inc. The anodes were composed of synthetic graphite (KS-6) from Timrex Inc. (average particle size ca. 6 μm, 90 wt.%), PVdF binder (10 wt.%) from Solvey Inc., and copper foil current collectors. The cathodes were comprised of $LiMn_2O_4$ powder from Merck KGaA (particle size of 5–10 μm, 75 wt.%), 15 wt.% graphite powder KS-6 (Timrex Inc.) as a conductive additive, 5 wt.% PVdF, 5 wt.% conductive carbon black, and an aluminum foil (Goodfellow,

* Corresponding author. Tel.: +972-3-5318317; fax: +972-3-5351250.
E-mail address: aurbach@mail.biu.ac.il (D. Aurbach).

0378-7753/03/$ – see front matter
doi:10.1016/S0378-7753(03)00256-8

England) current collector. Slurries containing the active mass and the binder were prepared using *N*-methyl pyrrolidone (Fluka Inc.) and were coated on the appropriate current collectors, as already described [6]. The electrodes were dried in an oven at 140 °C and were then transferred to the glove boxes. All the electroanalytical characterizations of the electrodes were performed in three-electrode cells based on standard coin-type cells (Model 2032, NRC Canada, ϕ 19 mm). A Li wire reference electrode was pasted on a nickel wire, which was placed between the working electrode and the Li counter-electrode foil, while being covered by the separator membrane (Celgard 2400). Long-term cycling tests for graphite and $LiMn_2O_4$ electrodes were performed in two-electrode standard coin-type cells, separated by a porous polypropylene membrane (Celgard Inc.). These cells were hermetically sealed in a dry air-filled glove box using the 2325 Coin Cell Crimper System (NRC, Canada).

A Maccor multichannel system (Model 2000) was used for prolonged galvanostatic cycling. For voltammetric measurements, an Arbin Inc. computerized multichannel battery tester and a computerized EG&G Model 273 potentiostat were used.

Impedance spectra were measured using the Autolab Model PGSTAT20 Electrochemical system and a frequency response analyzer (FRA) from Eco Chemie BV Inc., driven by a Pentium II IBM PC. The amplitude of the ac voltage was 3 mV and the impedance was measured at a constant base potential after the appropriate equilibration. FTIR measurements of pristine and cycled electrodes were carried out in diffuse reflectance mode using Magna 860 FTIR spectrometer (Nicolet Inc.), operating under H_2O and CO_2 free atmosphere (in a homemade glove box).

We used ARC (Arthur D Little Inc. Model 2000) with 5 °C increments at the rate of 2 °C/min in search for self-heating at the sensitivity threshold of 0.02 °C/min.

3. Results and discussion

Fig. 1 shows a family of cyclic voltammograms (CVs) of graphite electrodes cycled at the scan rate of 1 mV/s in LiFAP, $LiPF_6$ and LiBETI solutions (as indicated in the figure). The CVs reflect the usual irreversible reduction of solution species at potentials below 1.0 V, which form passivating surface films, and the reversible lithium insertion and deinsertion processes at potentials below 0.5 V (versus Li/Li^+). It is important to note that the first and subsequent CVs (see Fig. 1) related to the LiFAP solution are very similar in the Li insertion–deinsertion potential range (<0.5 V), while the CVs related to the $LiPF_6$ and LiBETI solutions change upon repeated cycling, and reach stability only after three to four subsequent cycles. Repeated voltammetric cycling of graphite electrodes revealed a faster kinetics of Li-ion insertion/deinsertion in LiFAP solutions compared to $LiPF_6$ solutions. This trend can be seen not only

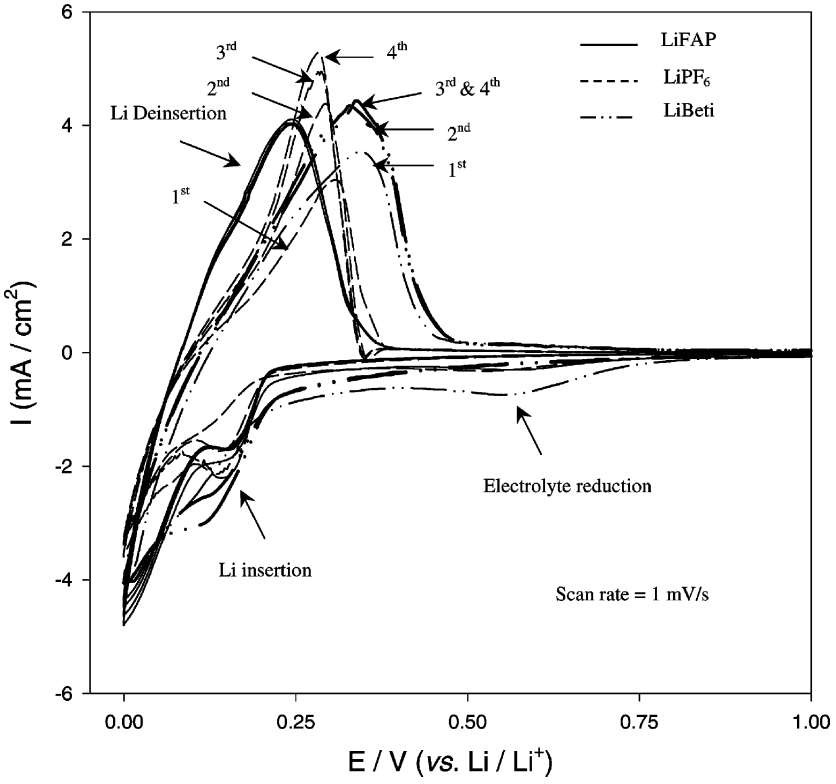

Fig. 1. Cyclic voltammograms of graphite electrodes at the scan rate of 1 mV/s at 30 °C (lithium as counter and reference electrodes). LiFAP, $LiPF_6$ and LiBETI solutions as indicated in the figure. The solid lines show the first cycle, while the dotted lines show the subsequent cycles.

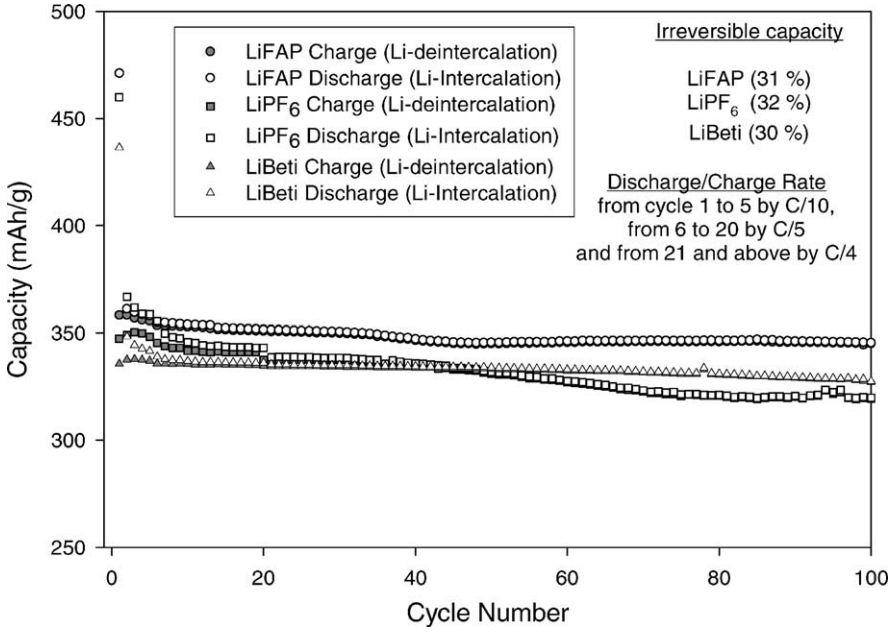

Fig. 2. Typical cycle life curves (capacity vs. cycle number) of graphite electrodes obtained in coin-type cell testing at 30 °C. Li metal counter electrodes, EC:DEC:DMC (2:1:2) 1 M LiFAP, $LiPF_6$, and LiBETI solutions as indicated. The rates for the charge and the discharge processes are as also indicated.

in fast-scan rate CV measurements but also in SSCV (i.e. at the μV/s range).

Fig. 2 compares cycling data (capacity versus cycle number curves) of graphite electrodes in three solutions containing LiFAP, $LiPF_6$, and LiBETI, as indicated. Both charge and discharge responses are presented (solid and dashed lines, as indicated, Li deinsertion–insertion processes, respectively). It is very significant that in the LiFAP solutions, the highest capacity and the best stability are achieved, while in $LiPF_6$ solutions the capacity-fading upon cycling is more pronounced (yet low) though the irreversible capacities are comparable in all of these solutions.

Fig. 3 shows typical Nyquist plots measured with stabilized graphite electrodes at two different equilibrium potentials related to stages I + II at 75 mV, and to a fully lithiated state (30 mV) in LiFAP, $LiPF_6$ and LiBETI solutions, as marked in the figure. The spectra include a high-medium frequency flat semicircle (more symmetrical with $LiPF_6$, and distorted with LiFAP and LiBETI solutions), and straight, linear Z'' versus Z' behavior at the low frequency. At the very low frequencies ($\omega \rightarrow 0$), the Z'' versus Z' lines become very steep. As already discussed in detail [7], the high-medium frequency semicircles in these spectra relate to the surface films, which cover the graphite electrodes, and their interface with the bulk carbon phase. The processes related to the high-medium frequency impedance, are Li-ion migration through the surface films and the Li-ion transfer across the film–carbon interface, coupled with the relevant capacitances (related to the surface films and to a double layer). At the low frequencies, the straight Z'' versus Z' lines (see Fig. 3) behave as 'Warburg'-type elements, and reflect solid state diffusion of Li-ions in the bulk graphite. The chemical diffusion coefficient of Li-ions in graphite as a function of potential and intercalation level can be calculated from this part of the impedance spectra [7]. At the very low frequencies, the steep, straight Z'' versus Z' plots show a nearly capacitive behavior, and thus reflect the accumulation of lithium in the graphite via phase transitions between Li intercalation stages [7]. It is very significant that the diameters of the semicircle in the Nyquist plots related to the LiBETI solutions are the smallest compared to that of LiFAP and $LiPF_6$ solutions while for LiFAP solutions, the high frequency impedance is higher than that related to $LiPF_6$ solutions (Fig. 3). The impedance of both Li and lithiated graphite electrodes is usually higher in $LiPF_6$/alkyl carbonate solutions than that measured in alkyl carbonate solutions with salts such as $LiAsF_6$, $LiClO_4$, $LiC(SO_2CF_3)_3$, etc. [8]. This is due to the fact that surface films formed on lithium and lithiated graphite electrodes in $LiPF_6$ solutions contain a high concentration of LiF formed by the reactions of both trace HF and PF_6^- anions on the active surfaces [8]. Surface films comprising LiF are highly resistive to Li-ion migration, much more than the surface films comprising organic or inorganic Li carbonates, which are formed by the reduction of the alkyl carbonates (in cases where the Li or Li–C surface chemistry is dominated by solvent reduction). We presume that LiFAP solutions contain much less HF than $LiPF_6$ solutions, and therefore, the surface films formed on lithiated graphite in the former solutions should contain less LiF, and hence should be less resistive than the surface films formed on graphite electrodes in the $LiPF_6$ solutions. Therefore, the impedance spectra in Fig. 3 that reflect a higher surface resistance of the graphite electrodes in the LiFAP solutions may indicate some involvement of the FAP^- anion

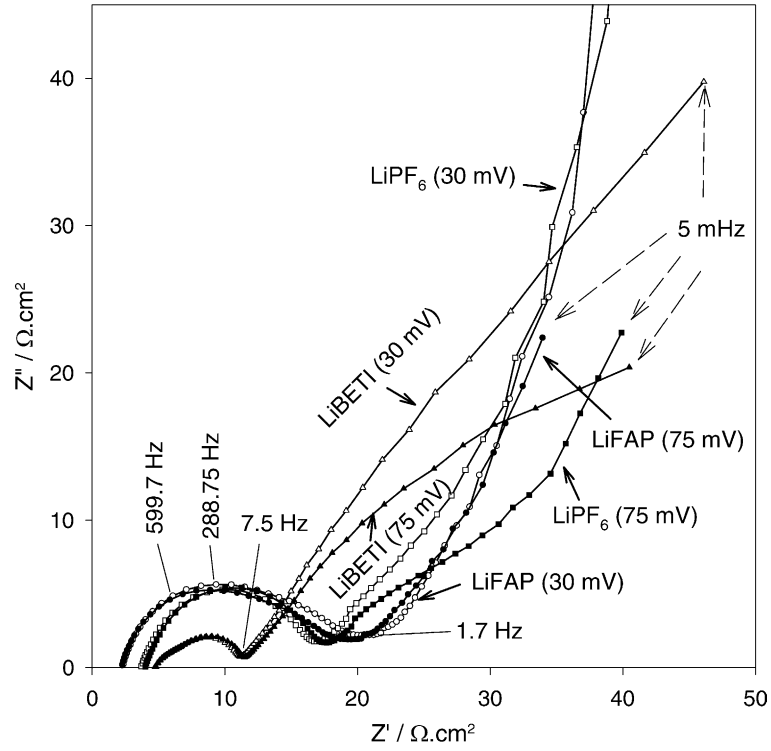

Fig. 3. Typical Nyquist plots obtained from graphite electrodes at two different equilibrium potentials (75 and 30 mV) in LiFAP, $LiPF_6$ and LiBETI solutions at 30 °C. These series of experiments were carried out after the electrodes were cycled (CV) in the potential range of interest, during which stable surface films were formed. Some frequencies are also marked near the spectra. The relevant potentials are indicated.

in the surface chemistry of the graphite electrodes in a way that stabilizes the electrode–solution interface, as is evident from the high performance of Li–graphite electrodes in the LiFAP solutions, but also increases the impedance of the surface films. The diameter of the semicircle (related to surface films) is much lower for LiBETI solutions compared to both $LiPF_6$ and LiFAP solutions as there is no HF contamination in LiBETI solutions and hence there is no formation of resistive LiF surface films on graphite electrodes in these solutions.

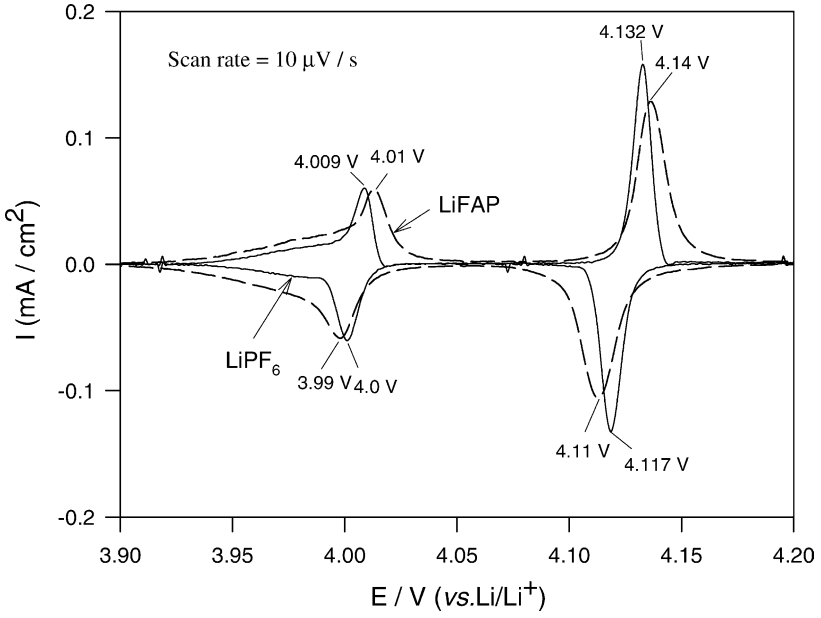

Fig. 4. Slow scan cyclic voltammograms (SSCV) of $LiMn_2O_4$ electrodes between 3.9 and 4.20 V at a scan rate of 10 μV/s (lithium as counter and reference electrodes) in LiFAP and $LiPF_6$ solutions as indicated.

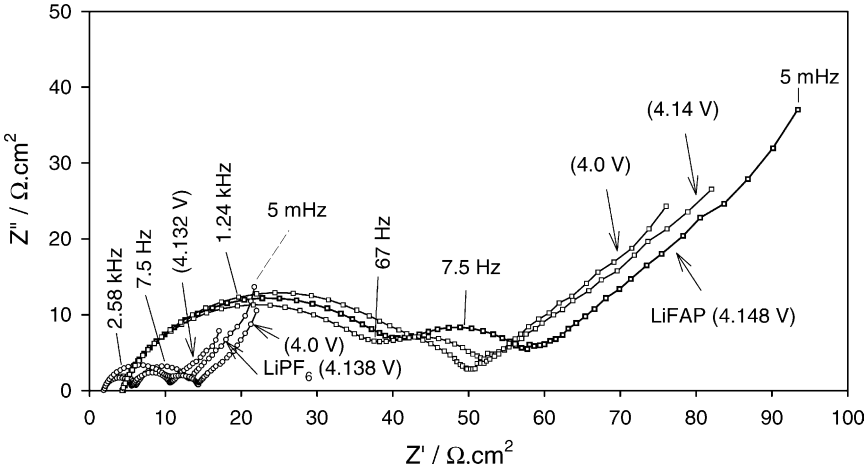

Fig. 5. Typical Nyquist plots at three different potentials (as indicated in the figure) measured with $LiMn_2O_4$ electrodes in LiFAP and $LiPF_6$ solutions at 30 °C. The electrodes were preliminarily equilibrated at the different potentials (as indicated) for at least 2–5 h before the EIS measurements.

Spectral studies of lithiated graphite electrodes by XPS and FTIR showed that the most abundant element on the electrode's surfaces treated in the $LiPF_6$ solutions is fluorine. The surface films formed on graphite electrodes in $LiPF_6$ solutions contain also ROLi species. In LiFAP and LiBETI solutions the major surface species formed are $ROCO_2Li$ species, products of the solvents reduction. In the case of $LiPF_6$ solutions direct reduction of trace HF and a possible secondary reaction of HF with the solvent reduction products (e.g. $ROCO_2Li + HF \rightarrow ROCO_2H + LiF$), as already described [8], have a very strong impact on the electrodes surface chemistry (which makes LiF to be a major component in the passivating surface films).

The difference in the surface chemistry in LiFAP, LiBETI and $LiPF_6$ solutions as described above, may explain the difference in the behavior of graphite electrodes in these three solutions, as presented in Figs. 1–3.

Fig. 4 shows slow scan-rate cyclic voltammograms (SSCV, 10 μV/s) of composite $LiMn_2O_4$ electrodes in LiFAP and $LiPF_6$ solutions (as indicated). The CVs in this figure reflect the highly reversible behavior of the $LiMn_2O_4$ electrodes in both solutions. The two Li insertion–deinsertion processes occurring around 4.0 V and 4.12 V (Li/Li^+) via first order phase transitions are clearly seen. In addition, upon cycling at 30 °C, a capacity-fading is measured in both solutions. However, there are two major differences in the electrochemical behavior of the $LiMn_2O_4$ electrodes in the two solutions: (a) The electrodes' capacity and stability (upon cycling) are higher in the LiFAP solutions. (b) The electrodes' kinetics are more sluggish in the LiFAP solutions, as is evident from the broader peaks in Fig. 4.

Fig. 5 shows typical Nyquist plots measured with stabilized $LiMn_2O_4$ composite electrodes during delithiation, at three equilibrium potentials corresponding to peak potentials in SSCV and completely delithiated state in LiFAP and $LiPF_6$ solutions, as indicated in the figure. In general, the impedance spectra of these electrodes in both solutions reflect the serial nature of Li insertion–deinsertion processes into $LiMn_2O_4$ electrodes, as already demonstrated and discussed in detail [7]. At the high-medium frequencies, two flat semicircles, which may be well separated (as in Fig. 5, $LiPF_6$ solutions) or superimposed (LiFAP solutions, Fig. 5), reflect Li migration through surface layers (the high frequency semicircle) and interfacial charge transfer (the medium semicircle). At the low frequencies, a 'Warburg'-type element (linear Z'' versus Z' behavior) in the spectra reflect the solid state diffusion of Li-ions into the bulk $LiMn_2O_4$ particles. A comparison between the impedance spectra in Fig. 5 clearly demonstrate that the electrodes' real component of impedance in $LiMn_2O_4$ is higher in LiFAP solutions, and the resolution of the spectra related to LiFAP solutions in the high-to-medium frequencies is lower. This means that the surface chemistry of the electrodes in both solutions is different. The real component of the impedance is higher for the electrodes in the LiFAP solutions correlates well with their more sluggish kinetics, as reflected by the voltammetric studies (Fig. 4). The surface chemistry that can be developed in the various solutions was studied by XPS and FTIR spectroscopy. It is significant that the electrodes treated in the $LiPF_6$ solution contain surface LiF. These spectral studies reflect different surface chemistry, which is developed on $LiMn_2O_4$ electrodes in the two solutions. Polymerization of the solvent molecule to derivatives of polyethylene oxide and polycarbonates occurs in LiFAP solutions. The difference in the surface chemistry explains the difference in the electrochemical behavior of the electrodes in the LiFAP and the $LiPF_6$ solutions.

It is clear that in the $LiPF_6$ solution, surface LiF is formed. In contrast to graphite electrodes where there is a constant driving force towards the formation of LiF, in the case of the cathode materials, LiF may be formed in a thin layer by decomposition of the salt to LiF and PF_5 on the cathode and/or by acid–base reactions between $LiMn_2O_4$ and HF. A sufficiently thin LiF layer may not impede Li-ion transport to the active mass, yet may inhibit to some extent the reactions of solvent molecules on the cathode material.

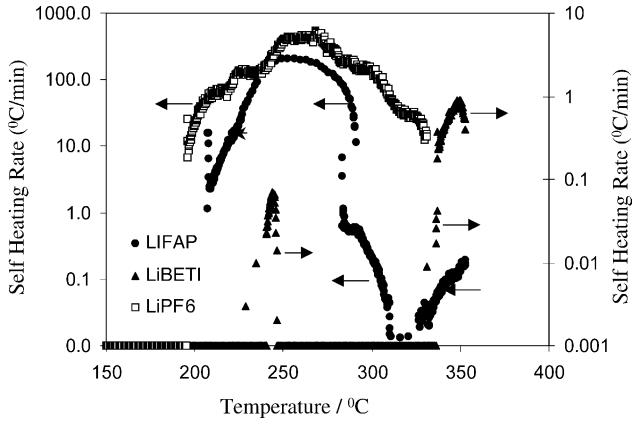

Fig. 6. Self-heating rates (SHR) vs. temperature for EC:DEC:DMC (2:1:2) 1 M solutions of LiFAP, $LiPF_6$ and LiBETI, measured by accelerating rate calorimetry (ARC).

However, other reactions between the active mass and species such as trace HF, which are unavoidably present in $LiPF_6$ solutions, may have a detrimental effect on the electrode's overall capacity. In LiFAP solutions, solvent reactions such as polymerization may take place, and hence, form resistive surface films (relatively high impedance, Fig. 5). However, these surface films, which impede Li-ion transport, may better protect the active mass from detrimental interactions with solution species. Thereby, the kinetics of $LiMn_2O_4$ cathodes are more sluggish in LiFAP solutions, but their capacity is higher.

The thermal stability of the solutions was studied by ARC. The highest thermal stability was found with the LiBETI solutions, which have the highest exothermic onset at 230 °C and the lowest self-heating rate (about of 1 °C/min) (Fig. 6). A small exotherm between 325 and 350 °C and one process with pressure development between 250 and 350 °C were detected upon heating LiBETI solutions (not presented). The thermal decomposition of the LiFAP solution starts at higher temperatures than that of $LiPF_6$ solutions (by 10 °C), however, the thermal reactions' rate of the LiFAP solutions is considerably higher (Fig. 6).

Fine examination of the thermal response (Fig. 6) of both $LiPF_6$ and LiFAP solutions reveals about five different processes reflected by SHR versus T plots. It should be noted that the thermal reactions of the least stable $LiPF_6$ solutions start in fact around 170 °C. These reactions are endothermic and generate gaseous products (HF, CO_2, PF_5, etc.), which develop high pressure. The onset for the first exothermic process of $LiPF_6$ solutions is 200 °C and for the second one is 220 °C.

4. Conclusion

The new salt LiFAP in ternary mixtures of EC, DEC and DMC seems to be very promising for use in rechargeable Li-ion batteries compared to $LiPF_6$ or LiBETI. Both graphite and $LiMn_2O_4$ electrodes behave better with LiFAP solutions in terms of reversibility and stability upon cycling than with $LiPF_6$ or LiBETI solutions. The difference in performance is due to the different surface chemistry developed in the various solutions, e.g. in $LiPF_6$ solutions, HF and PF_6^- anion reactions dominate the surface chemistry while in LiFAP solutions the surface chemistry relates mostly to solvent reactions. The scale of the thermal stability was found to be LiBETI > LiFAP > $LiPF_6$ solutions.

Acknowledgements

Partial support for this work was obtained from the BMBF, the German Ministry of Science, in the framework of the DIP program for Collaboration Between Israeli and German Scientists.

References

[1] J.O. Besenhard, M. Winter, Chem. Phys. Chem. 3 (2002) 155.
[2] E. Sloop, J.K. Pugh, S. Wang, J.B. Kerr, K. Kinoshita, Electrochem. Solid State Lett. 4 (2001) A42.
[3] A.M. Andersson, K. Edstrom, J. Electrochem. Soc. 148 (2001) A1100.
[4] K. Kanamura, S. Shiraishi, Z.I. Takehara, J. Electrochem. Soc. 143 (1996) 2187.
[5] M. Schmidt, U. Heider, A. Kuehner, R. Oesten, M. Jungnitz, N. Ignatev, P. Sartori, J. Power Sources 97–98 (2001) 557.
[6] J.S. Gnanaraj, M.D. Levi, E. Levi, G. Salitra, D. Aurbach, J.E. Fischer, A. Claye, J. Electrochem. Soc. 148 (2001) A525.
[7] D. Aurbach, M.D. Levi, J. Phys. Chem. B 101 (1997) 4641.
[8] D. Aurbach, B. Markovsky, A. Schechter, Y. Ein-Eli, H. Cohen, J. Electrochem. Soc. 143 (1996) 3809.